ACS OMEGA

http://pubs.acs.org/journal/acsodf
Article

Biochemical and Structural Analysis of the Bacterial Enzyme Succinyl-Diaminopimelate Desuccinylase (DapE) from *Acinetobacter baumannii*

Emma H. Kelley,[#] George Minasov,[#] Katherine Konczak, Ludmilla Shuvalova, Joseph S. Brunzelle, Shantanu Shukla, Megan Beulke, Teerana Thabthimthong, Kenneth W. Olsen, Nicole L. Inniss, Karla J. F. Satchell, and Daniel P. Becker*

Cite This: *ACS Omega* 2024, 9, 3905−3915

Read Online

ACCESS | Metrics & More | Article Recommendations | Supporting Information

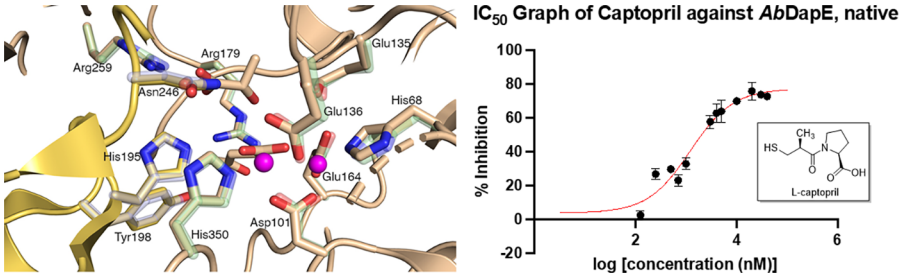

ABSTRACT: There is an urgent need for new antibiotics given the rise of antibiotic resistance, and succinyl-diaminopimelate desuccinylase (DapE, E.C. 3.5.1.18) has emerged as a promising bacterial enzyme target. DapE from *Haemophilus influenzae* (*Hi*DapE) has been studied and inhibitors identified, but it is essential to explore DapE from different species to assess selective versus broad-spectrum therapeutics. We have determined the structure of DapE from the ESKAPE pathogen *Acinetobacter baumannii* (*Ab*DapE) and studied inhibition by known inhibitors of *Hi*DapE. *Ab*DapE is inhibited by captopril and sulfate comparable to *Hi*DapE, but *Ab*DapE was not significantly inhibited by a known indoline sulfonamide *Hi*DapE inhibitor. Captopril and sulfate both stabilize *Hi*DapE by increasing the thermal melting temperature (T_m) in thermal shift assays. By contrast, sulfate decreases the stability of the *Ab*DapE enzyme, whereas captopril increases the stability. Further, we report two crystal structures of selenomethionine-substituted *Ab*DapE in the closed conformation, one with *Ab*DapE in complex with succinate derived from enzymatic hydrolysis of N^6-methyl-L,L-SDAP substrate and acetate (PDB code 7T1Q, 2.25 Å resolution), and a crystal structure of *Ab*DapE with bound succinate along with L-(S)-lactate, a product of degradation of citric acid from the crystallization buffer during X-ray irradiation (PDB code 8F8O, 2.10 Å resolution).

INTRODUCTION

The growing threat from antibiotic-resistant bacterial strains[1] underscores the need to discover antibiotics with new mechanisms of action. The most widely encountered virulent species of antibiotic multidrug-resistant (MDR) microorganisms seen worldwide are known as the ESKAPE pathogens, which consist of *Enterococcus faecium*, *Staphylococcus aureus*, *Klebsiella pneumoniae*, *Acinetobacter baumannii*, *Pseudomonas aeruginosa*, and *Enterobacter spp*.[2] The ESKAPE pathogens are becoming increasingly resistant to many broad-spectrum antibiotics that are currently available due to a range of resistance mechanisms including mutations of the drug target, the use of efflux pumps, the ability to inactivate specific drugs, reduced cellular membrane permeability, and the growth of biofilms when the microbe becomes dormant in the host.[2] *A. baumannii* is an opportunistic bacterial pathogen[3] primarily associated with hospital-acquired infections, but also plagues military personnel returning from conflict zones. Given that *A. baumannii* now exhibits a high incidence of MDR strains, there is an urgent need to develop novel and effective antibacterial agents against this pathogen.

The L-lysine biosynthetic pathway provides a wealth of opportunities toward new antibiotic targets, as it is required for bacterial growth and survival but is absent in humans.[4] In particular, *dapE*-encoded *N*-succinyl-L,L-diaminopimelic acid desuccinylase (DapE, E.C. 3.5.1.18) is present in all Gram-negative and most Gram-positive bacteria and is one enzyme of

Received: October 19, 2023
Revised: November 23, 2023
Accepted: November 24, 2023
Published: January 8, 2024

Scheme 1. Hydrolysis of L,L-SDAP and a substrate analogue by DapE[a]

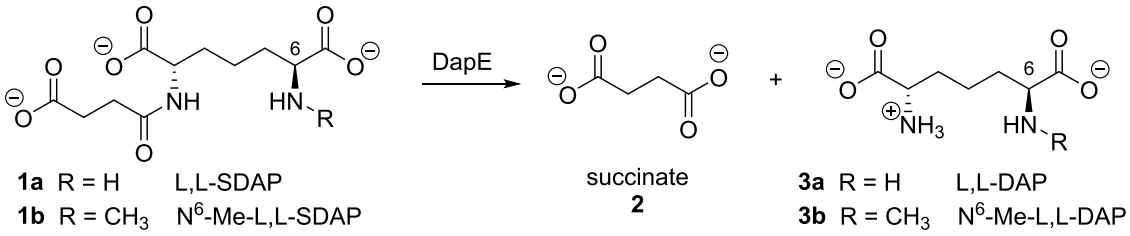

[a]L,L-SDAP endogenous substrate (**1a**) and assay substrate N^6-methyl-L,L-SDAP7 (**1b**) with formation of hydrolysis products succinate (2) and L,L-diaminopimelic acid derivatives **3a** and **3b**, respectively.

the L-lysine biosynthetic pathway that is underexplored as a potential drug target.[5] DapE is responsible for the synthesis of both lysine and *meso*-diaminopimelate (*m*-DAP),[6] both of which are critical for peptidoglycan cell-wall synthesis. DapE catalyzes the hydrolysis of the substrate *N*-succinyl-L,L-diaminopimelic acid (L,L-SDAP), releasing succinate and providing L,L-diaminopimelic acid (L,L-DAP, Scheme 1).[7]

Knockout of *dapE* is lethal to *Helicobacter pylori* and *Mycobacterium smegmatis*, revealing the essential role of this enzyme in bacterial survival.[8,9] The lack of a similar pathway in humans suggests that inhibition of DapE should be selectively toxic to bacteria, making it a promising antibiotic target with a new mechanism of action.[5] We previously reported an assay[7] to assess inhibition of DapE employing the synthetic substrate N^6-methyl-L,L-SDAP (**1b**), which when cleaved by DapE affords the primary amine product **3b** (Scheme 1) that is quantified spectrophotometrically after treatment with ninhydrin.

The first X-ray crystal structure of an apo DapE from *Neisseria meningitidis* (*Nm*DapE) was solved in 2005,[10] and structures of mono- and dizinc forms from *Haemophilus influenzae* (*Hi*DapE)[11] and *Nm*DapE[12] were reported thereafter, including a structure of the DapE inhibitor captopril[13] bound to the active site of *Nm*DapE.[12] We reported a DapE crystal structure revealing the previously unknown closed conformation of dimeric DapE with the products of enzymatic cleavage, succinate and diaminopimelic acid, bound in the *Hi*DapE active site (PDB 5VO3).[14] Interestingly, this substantial DapE conformational change was predicted prior to the report of the crystal structure by the elegant computational work of Mishra who employed principal component analysis of molecular dynamics trajectories of the DapE apo enzyme and the DapE-SDAP complex.[15] Thereafter, we reported an atomic-resolution (1.3 Å) structure of the open conformation of *Nm*DapE (PDB 5UEJ.)[16] These DapE structures have enabled refinement of the understanding of the enzymatic mechanism of hydrolysis of DapE and further insight into the design of successful inhibitors toward new antibiotics.

Herein, we report the inhibition of *Ab*DapE by captopril and sulfate using our ninhydrin-based assay and the effect of these compounds on the thermal melting temperature (T_m) of *Ab*DapE proteins using thermal shift assays. We report a lack of inhibition of *Ab*DapE by a synthetic micromolar inhibitor of *Hi*DapE, indoline sulfonamide. Furthermore, we report two X-ray crystal structures of *Ab*DapE in the closed conformation. Co-crystallization of *Ab*DapE with the modified substrate N^6-Me-L,L-SDAP, allowed us to capture the enzyme in the closed conformation in complex with succinate.

MATERIALS AND METHODS

All chemicals were purchased from commercial sources and were of the highest quality available.

Preparation of Selenomethinoine and Native DapE Proteins. *Ab*DapE was expressed in *Escherichia coli* and prepared according to a general protocol described previously.[7,12,14] For protein crystallography and enzymatic characterization, bacteria were cultured in selenomethionine (SeMet) and M9-minimal media, respectively. Media were supplemented with 150 μg/mL ampicillin at 37 °C with shaking at 210 rpm until the OD_{600} reached a value of 1.5. The temperature was lowered to 18 °C, and isopropyl-D-thiogalactopyranoside (IPTG) was added to a final concentration of 0.5 mM. The culture was grown for 18 h and then centrifuged at 4,500 rpm for 10 min at 4 °C. The cell pellet derived from 3 L of culture was resuspended in 150 mL (1 g of cells/5 mL of buffer) of lysis buffer (10 mM Tris-HCl, pH 8.3), 500 mM NaCl, 5% glycerol, 20 mM imidazole, 5 mM tris (2-carboxyethyl) phosphine hydrochloride (TCEP) and stored at −30 °C. A frozen suspension of cells with expressed protein was thawed and sonicated at 50% amplitude in 5 s × 10 s cycles for 20 min at 4 °C. The lysate was cleared by centrifugation at 18,000*g* for 40 min at 4 °C, the supernatant was collected, and the protein was purified as previously described with some modifications. The supernatant was loaded onto a His-Trap FF (Ni-NTA) column using a GE Healthcare ÅKTA Pure system with a loading buffer (10 mM Tris-HCl (pH 8.3), 500 mM NaCl, 1 mM TCEP, and 5% glycerol). The column was washed with loading buffer followed by 10 mM Tris-HCl (pH 8.3), 500 mM NaCl, and 25 mM imidazole, and the protein was eluted with 10 mM Tris-HCl (pH 8.3), 500 mM NaCl and 500 mM imidazole. Eluate was loaded onto a Superdex 200 26/600 column and eluted with a loading buffer. Pure protein was collected and incubated with tobacco etch virus (TEV) protease overnight in buffer (10 mM Tris-HCl, pH 8.3, and 500 mM NaCl). The cleaved tag and TEV protease were separated from the protein by Ni-NTA-affinity chromatography using the loading buffer, and DapE protein was collected in two separate fractions: the flowthrough fraction and that with 25 mM imidazole in the loading buffer. Both fractions contained pure protein but were kept separate. Prior to crystallization, the protein was dialyzed into 150 mM NaCl, 10 mM Tris-HCl (pH 8.3), and 0.1 mM $ZnCl_2$ for 3 h at room temperature. The protein was concentrated to 6−11 mg/mL, portions of which were incubated with 2 mM N^6-methyl-L,L-SDAP for 30 min at room temperature and used for crystallization trials immediately or frozen in liquid nitrogen and kept at −80 °C for future use.

https://doi.org/10.1021/acsomega.3c08231
ACS Omega 2024, 9, 3905−3915

Crystallization and Structure Determination. Crystallizations were set up with freshly purified *Ab*DapE-SeMet protein at various concentrations of 6−11 mg/mL in 150 mM NaCl, 10 mM Tris-HCl (pH 8.3), and 2 mM N^6-Me-L,L-SDAP using the sitting drop method in Corning 96-well plates with Classics II, PEGs II and Anions crystallization screens (QIAGEN) at 20 °C.

Diffraction quality crystals were screened, and data sets were collected at the 21-ID-G and 21-ID-D beamline of the Life Science Collaborative Access Team (LS-CAT) at the Advanced Photon Source, Argonne National Laboratory. Images were indexed, integrated, and scaled using the HKL3000 suite.[17] Structures were determined by Molecular Replacement using Phaser[18] from the CCP4 Suite.[19] The crystal structure of the DapE from *N. meningitidis* MC58 (PDB code 5UEJ) was used as a search model. Initial solutions were refined in REFMAC,[20] and manual model corrections were made in Coot.[21] At this point, structures were carefully examined, and the two with the highest resolution and the best quality electron density maps near the substrate binding sites were selected for further refinement. Water molecules were generated using ARP/wARP,[22] and ligand molecules were fit into electron density maps in Coot. Structures were further refined in REFMAC, and TLS corrections were applied during the final stages of refinement. Molprobity[23,24] was used for monitoring the quality of the model during refinement and for the final validation of the structure. X-Ray data quality and structure refinement statistics are listed in Table S1. Coordinates of the final models and experimental structure factors for *Ab*DapE-SeMet/succinate and *Ab*DapE-SeMet/succinate + L-(S)-lactate complexes were deposited in the Protein Data Bank (PDB) as PDB entries 7T1Q and 8F8O, respectively.

Enzyme assay. A discontinuous kinetic assay was performed utilizing a Techne PCR Thermal Cycler System with a modified ninhydrin assay protocol.[7] The volume of each component was adjusted to fit a total reaction volume of 100 μL. The final potential inhibitor concentration was 5 μM for captopril and 5 mM for Li_2SO_4. One indoline sulfonamide *Hi*DapE inhibitor was assayed for inhibition of *Ab*DapE at 100 μM. Inhibitors were dissolved in neat dimethylsulfoxide (DMSO, stock stored at −10 °C), and the preassay concentrations were adjusted to give a final concentration of 5% DMSO in the assay. The final *Ab*DapE or *Hi*DapE concentration was 8 nM. To a 50 mM HEPES (pH 7.5) buffered solution at 30 °C was added the selected inhibitor followed by *Ab*DapE or *Hi*DapE and incubated for 10 min. N^6-Methyl-L,L-SDAP (2 mM) was added, and the mixture was allowed to react for 10 min followed by heating at 100 °C for 1 min and cooling to 0 °C. A 2% ninhydrin solution (100 μL) was added, and the mixture was vortexed or mixed well by rapid pipetting while cooled at 0 °C. The reaction was then heated at 80 °C for 15 min. The absorbance of an 80 μL aliquot was recorded at 570 nm on a BioTek Synergy 2 microplate reader.

Kinetic studies. A discontinuous kinetic assay was performed utilizing a Techne PCR Thermal Cycler System with a modified ninhydrin assay protocol.[7] The volume of each component was adjusted to fit the total reaction volume of 100 μL, and the final enzyme concentration was 8 nM. Inhibition of *Ab*DapE or *Hi*DapE with various concentrations of inhibitor was studied in triplicate while changing the substrate concentration from 0.5 to 6.0 mM. The amount of enzymatic product N^6-Me-L,L-DAP that was formed over 10 min was monitored by measuring the absorbance of the complex formed from the reaction of N^6-Me-L,L-DAP with 2% ninhydrin in a similar fashion as stated above. The enzymatic activity was reported as the rate of formation of the product N^6-Me-L,L-DAP in velocity (mM/sec). The kinetic constants (K_i) were found using the Michaelis−Menten equation in Microsoft Excel and GraphPad Prism using a nonlinear regression.

DapE Enzyme Inhibition: K_i Determination. The inhibition of *Ab*DapE and *Hi*DapE by captopril and sulfate was assessed following the protocol detailed by us previously[7] with modifications as detailed above. The formation of N^6-Me-L,L-DAP was detected by measuring the change in absorbance at 570 nm, which was then converted into velocity by finding the path length of the well-plate using a compound with a known molar absorption coefficient (ascorbic acid, ε = 2.8 mM^{-1} cm^{-1})[25] at a known compound concentration, 80 mM. Once the path length was found, the absorbance was converted into velocity using nonlinear regression and the K_i values were determined using Microsoft Excel and GraphPad Prism.

Determination of k_{cat}/K_M with *Ab*DapE. A discontinuous kinetic assay was performed utilizing a Techne PCR Thermal Cycler System with a modified ninhydrin assay protocol.[7] The volume of each component was adjusted to fit the total reaction volume of 100 μL, and the final enzyme concentration was 8 nM. The activities of *Ab*DapE and *Hi*DapE were assessed by changing the substrate concentration from 0 mM to 6.5 mM. The amount of enzymatic product N^6-Me-L,L-DAP that was formed over 10 min was monitored by measuring the absorbance of the complex formed from the reaction of N^6-Me-L,L-DAP with 2% ninhydrin in a similar fashion as stated above. The enzymatic activity was reported as the rate of formation of the product, N^6-Me-L,L-DAP, in velocity (mM/sec). The kinetic constants (k_{cat}/K_M) were found by using GraphPad Prism using a nonlinear regression using the Michaelis−Menten model.

Sequence Comparisons. The nonrepetitive sequence database was searched for homologues of *Hi*DapE using the blastp algorithm.[26] The sequences for the fiveDapE proteins found were aligned using the Clustal Omega algorithm[27] and ESPript (Figure S9).[28]

Thermal Shift Assay. Thermal shift studies were conducted on a Step One Real-Time PCR System and the associated QuantStudio software. Protein denaturation was measured by detecting the change in fluorescence of the SYPRO Orange dye. *Hi*DapE was used at a final concentration of 200 nM, and SYPRO Orange was used at a final concentration of 10X. *Ab*DapE-native enzyme was used at a final concentration of 16 μM and 10× SYPRO Orange dye. The *Ab*DapE-SeMet was tested at a final concentration of 6 μM and SYPRO Orange was used at a final concentration of 10×. There was no change in T_m or inhibition by DMSO if the concentration of DMSO was kept lower than 5%. Dye concentrations higher than 12× denatured the enzyme. The experiment was carried out in 10-μL triplicates in 50 mM HEPES buffer at pH 7.5 in nanopure water, and the inhibitor concentrations were selected based on the half-maximal inhibitory concentration (IC_{50}) values of the inhibitor. Sample solutions were dispensed into a 96-well optical reaction plate (Thermo Fisher Scientific), and the plate was sealed with an optical PCR plate sheet (Thermo Fisher Scientific). After equilibrating the system for 2 min at 25 °C, the temperature

https://doi.org/10.1021/acsomega.3c08231
ACS Omega 2024, 9, 3905−3915

Table 1. Inhibition of *Hi*DapE and *Ab*DapE

Inhibitor	Structure	*Hi*DapE		*Ab*DapE
		K_i (μM)	IC_{50} (μM)[a]	IC_{50} (μM) or % inhibition
Captopril	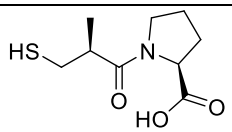	1.82 ± 0.09[b]	3.3[b]	1.22 ± 0.60
1-acetyl-5-chloro-N-isopentylindoline-6-sulfonamide	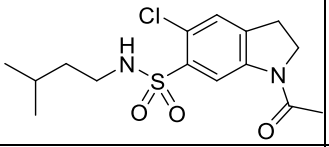	ND[c]	54[d]	2.98 ± 0.74% at 100 μM
Lithium sulfate	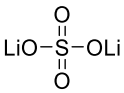	23,900 ± 5,900	ND	13,500 ± 1,100[e]

[a]Determined with N^6-methyl-L,L-SDAP substrate in the DapE ninhydrin assay.[7] [b]Captopril values taken from the literature.[30] [c]Not determined. [d]Standard deviation was not reported in the literature.[31] [e]Assayed at 5 mM.

was continuously increased at a rate of 0.05 °C/s for 25 min and finally maintained at 99 °C for 2 min. The samples were scanned from 330 to 350 nm every 8 s (0.4 °C). Melting curves were obtained from the negative derivative and exported from the instrument to Microsoft Excel. The negative first derivatives of the melting curves were differentiated into the third derivative. T_m values were plotted against the log [concentration], and the K_i values were calculated using a derived Van't Hoff equation according to Bhayani.[29]

RESULTS AND DISCUSSION

Enzyme Characterization and Inhibitors of *Ab*DapE. We determined that N^6- methyl-L,L-SDAP can serve as a substrate for *Ab*DapE, and it has a $k_{cat}/K_M = 3.4 \pm 0.9 \times 10^5$ $M^{-1}s^{-1}$ (Figure S1) compared to the $k_{cat}/K_M = 4.4 \pm 0.2 \times 10^5$ $M^{-1}s^{-1}$ (Figure S2) for the hydrolysis of *N*-methyl-L,L-SDAP by *Hi*DapE, thus the N^6-methyl modified substate is turned over at the same rate by both *Ab*DapE native enzyme and *Hi*DapE. We also assayed the SeMet derivative of *Ab*DapE (*Ab*DapE-SeMet) for hydrolysis of N^6-methyl-L,L-SDAP and found that the k_{cat}/K_M of *Ab*DapE-SeMet is $4.6 \pm 0.98 \times 10^5$ $M^{-1}s^{-1}$ (Figure S3), which is not statistically different.

To compare inhibition of *Ab*DapE to *Hi*DapE, we ran kinetic assays using our modified ninhydrin assay[7] using three known inhibitors of *Hi*DapE: captopril[30] lithium sulfate (Li_2SO_4),[16] and the indoline sulfonamide 1-acetyl-5-chloro-*N*-isopentylindoline-6-sulfonamide.[31] We found that both captopril and sulfate are competitive inhibitors of *Ab*DapE, as previously shown for *Hi*DapE.[16,30] Captopril inhibited *Ab*DapE with an IC_{50} of 1.2 μM versus an IC_{50} of 3.3 μM against *Hi*DapE (Table 1). The saturation curves are reported in the Supporting Information as Figures S4A−D. Thus, we observed that captopril is a single-digit μM inhibitor of *Ab*DapE, similar to *Hi*DapE. Surprisingly, we found that the indoline sulfonamide, 1-acetyl-5-chloro-*N*-isopentylindoline-6-sulfonamide, did not inhibit *Ab*DapE significantly at 100 μM, although this compound inhibits *Hi*DapE with an IC_{50} = 54.0 μM.[31] The lower potency of this inhibitor toward *Ab*DapE relative to its inhibition of *Hi*DapE is surprising and underscores the challenge of synthesizing a broad-spectrum DapE inhibitor. Sulfate inhibits *Ab*DapE with an IC_{50} of 13,500 μM, compared to the reported[16] K_i of 23,900 μM for*Hi*DapE.

Thermal Shift Assay (TSA) Results of *Hi*DapE, *Ab*DapE, and *Ab*DapE-SeMet. A thermal shift assay (TSA) was conducted to observe the T_m of DapE from *H. influenzae* and *A. baumannii*. As the indoline sulfonamide did not inhibit *Ab*DapE, we focused on the *Hi*DapE inhibitors captopril[30] and sulfate (Li_2SO_4).[16] In the absence of inhibitor, the melting curves of *Hi*DapE exhibit two melting temperatures, (T_m1) at 51.5 °C and (T_m2) at 78.2 °C, as does *Ab*DapE, (T_m1) at 41.9 °C and (T_m2) at 63.2 °C, both of which are notably lower temperatures. As we had *Ab*DapE-SeMet for the X-ray structure work, we also measured its T_m and compared it with the native enzyme. *Ab*DapE SeMet exhibited only one T_m at 65.2 °C. The significantly higher T_m relative to T_m1 for *Hi*DapE and for *Ab*DapE demonstrates the stabilizing effect of the SeMet, consistent with observation in the literature.[32]

Using the thermal shift data, we determined the K_i values for the inhibitors using a derived Van't Hoff Equation[29] and plotting the T_m vs log [concentration]. The thermal shifts occurred at concentrations very near the K_i values of the inhibitors for *HiDapE* and *AbDapE* reported for kinetic assays using the ninhydrin assay. Captopril and sulfate bind to *Hi*DapE with K_i values of 0.68 and 18,400 μM, respectively, and this thermal shift data are in agreement with previously published results determined via enzyme inhibition for *Hi*DapE, the reported K_i = 1.82 μM, and the IC_{50} for inhibition of *Hi*DapE by sulfate was 13,800 ± 2,800 μM.[16,30] The K_i found by the thermal shift for captopril versus *Ab*DapE was 0.79 μM, comparable to the K_i of 0.68 μM for captopril versus *Hi*DapE (Table 2).

X-ray Crystal Structure of DapE from *A. baumannii*. We crystallized *Ab*DapE-SeMet in the presence of the N^6-methyl-L,L-SDAP substrate, which yielded two structures of *Ab*DapE-SeMet in complex with a product of N^6-methyl-L,L-SDAP hydrolysis, succinic acid (crystal 1, PDB code 7T1Q), and with succinic acid and lactic acid (crystal 2, PDB code 8F8O). Both crystals belong to space group $P2_12_12_1$ with similar unit cell parameters (Table S1). Both structures were solved by using molecular replacement. The coordinates of *Nm*DapE (PDB code 5UEJ) were used to solve the structure of crystal 1 (7T1Q), and this refined model of *Ab*DapE-SeMet was used to solve the structure of crystal 2 (8F8O). Each

https://doi.org/10.1021/acsomega.3c08231
ACS Omega 2024, 9, 3905−3915

Table 2. Melt Temperatures from the Thermal Shift studies for *Hi*DapE and *Ab*DapE in the Absence and Presence of the Inhibitors Captopril and Lithium Sulfate

experiment	T_m1 *Hi*DapE[a] (°C)	K_i (μM)	T_m2 *Hi*DapE[a] (°C)	T_m1 *Ab*DapE[b] (°C)	T_m2 *Ab*DapE[b] (°C)	K_i (μM)	T_m *Ab*DapE-SeMet[c] (°C)	K_i (μM)
enzyme only	51.5 ± 0.3		78.2 ± 0.1	41.9 ± 0.3	63.2 ± 0.4		65.2 ± 0.1	
[Captopril]								
0.005 μM	51.5 ± 0.1		78.2 ± 0.1	41.9 ± 0.1	62.9 ± 0.1		65.3 ± 0.2	
0.05 μM	50.2 ± 0.6		78.6 ± 0.1	41.9 ± 0.2	63.3 ± 0.7		65.5 ± 0.1	
0.1 μM	50.0 ± 0.8		78.1 ± 0.1	41.9 ± 0.1	62.6 ± 0.3		65.3 ± 0.2	
0.5 μM	50.5 ± 0.1		78.3 ± 0.1	41.9 ± 0.2	63.1 ± 0.4		65.1 ± 0.1	
0.8 μM	50.3 ± 0.5	0.68 ± 0.65	77.9 ± 0.1	41.9 ± 0.1	62.3 ± 0.1	0.79 ± 0.61	66.1 ± 0.1	
1 μM	51.2 ± 0.2		77.8 ± 0.1	41.7 ± 0.1	63.4 ± 1.0		65.7 ± 0.1	
3 μM	52.2 ± 0.1		78.0 ± 0.1	41.7 ± 0.2	65.1 ± 0.3		66.4 ± 0.3	
5 μM	53.2 ± 0.2		77.8 ± 0.1	41.4 ± 0.1	64.1 ± 0.2		67.2 ± 0.2	9.4 ± 0.3
10 μM	52.9 ± 0.6		77.9 ± 0.1	41.1 ± 0.1	66.6 ± 0.2		68.5 ± 0.1	
15 μM				42.0 ± 0.1	65.5 ± 0.4			
[Li_2SO_4]								
0.001 mM	51.7 ± 0.3		75.6 ± 0.3	41.4 ± 0.1	63.1 ± 0.1		64.2 ± 0.7	
0.005 mM	51.4 ± 0.2		76.2 ± 0.5	41.8 ± 0.2	62.8 ± 0.2		64.1 ± 0.3	
0.1 mM	52.7 ± 0.4		76.1 ± 0.6	41.6 ± 0.1	62.2 ± 0.1		64.0 ± 0.2	
0.5 mM	51.2 ± 0.7		78.3 ± 0.1	41.7 ± 0.1	63.1 ± 0.1		64.9 ± 0.1	
1 mM	50.7 ± 0.2		77.8 ± 0.1	41.3 ± 0.1	63.0 ± 0.1		64.7 ± 0.5	
5 mM	51.2 ± 0.6		77.7 ± 0.1	41.6 ± 0.1	61.5 ± 0.2		65.2 ± 0.1	
10 mM	51.2 ± 0.6	18,400 ± 620	77.4 ± 0.1	41.5 ± 0.1	60.4 ± 0.1		65.0 ± 0.3	
30 mM	52.6 ± 0.5		74.6 ± 0.3	42.2 ± 0.2	59.1 ± 0.2			
50 mM	53.3 ± 0.5		75.9 ± 0.1	42.1 ± 0.1	58.3 ± 0.1		63.1 ± 0.1	
60 mM	53.3 ± 0.3		73.8 ± 0.1	42.4 ± 0.2	57.5 ± 0.1			
70 mM	54.4 ± 0.5		76.6 ± 0.1	42.4 ± 0.3	56.7 ± 0.2		61.8 ± 0.1	

[a]200 nM *Hi*DapE + 10× dye. [b]16 μM *Ab*DapE + 10× dye. [c]6 μM *Ab*DapE + 10× dye.

https://doi.org/10.1021/acsomega.3c08231
ACS Omega 2024, 9, 3905−3915

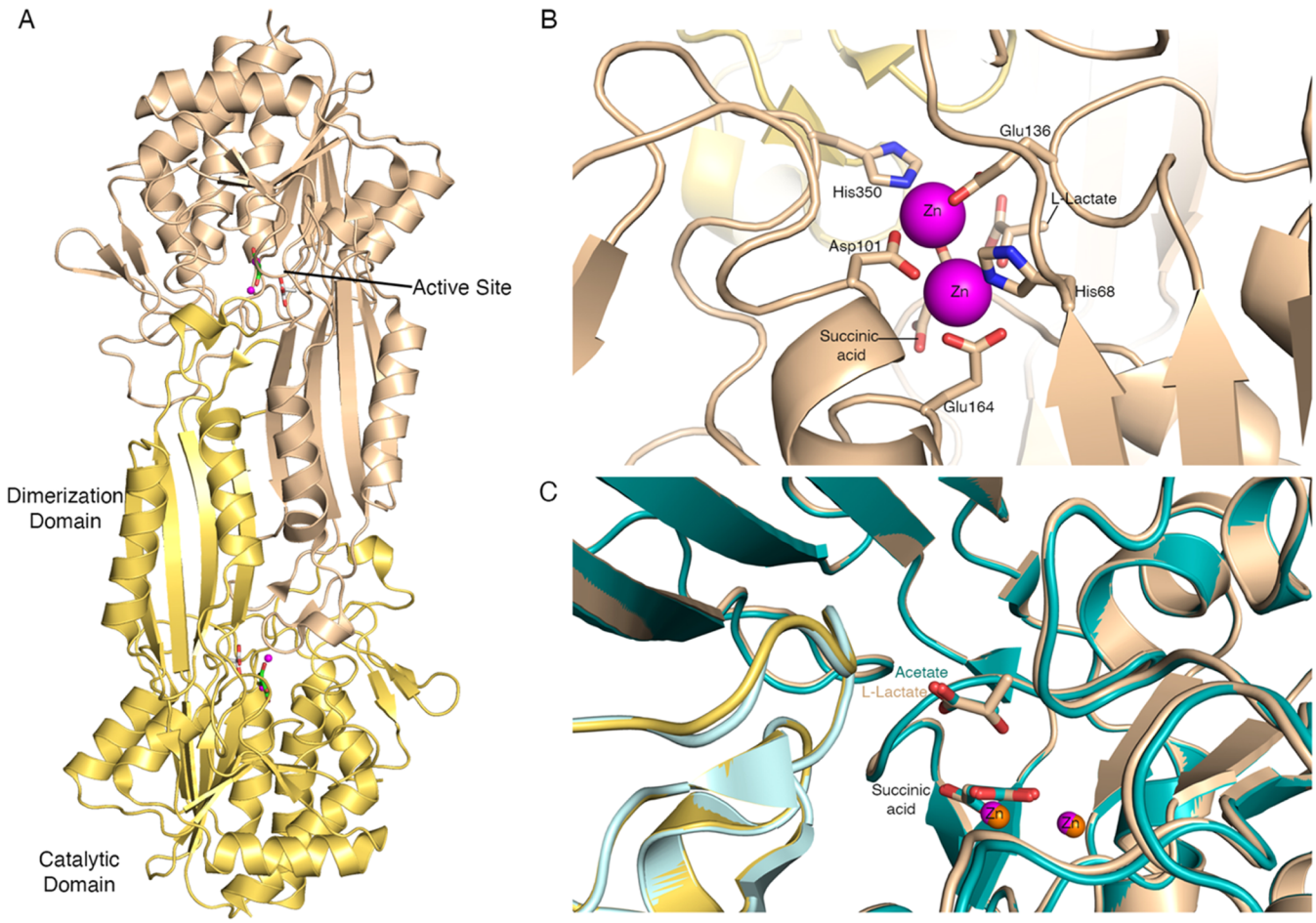

Figure 1. The structure of *A. baumannii* DapE-SeMet. (A) Overall structure of the *Ab*DapE-SeMet dimer from crystal 2 (PDB code 8F8O). Chain A is colored wheat, chain B yellow, and active site zinc ions are magenta. Atoms of the succinic acid (lime green carbons) and L-(S)-lactate (light gray carbons) are colored oxygen in red and nitrogen in blue. (B) Zoomed-in view of the zinc-binding site from chain A with atoms colored as in (A). Zinc-coordinating residues are shown as sticks. Atoms of succinic acid and L-(S)-lactate are also colored carbon in wheat, oxygen in red, and nitrogen in blue. (C) Superposition of the *Ab*DapE-SeMet structure of crystal 2 (8F8O, chain A in wheat, chain B in yellow) and the structure of crystal 1 (7T1Q, chain A in teal, chain B in cyan) active sites. Succinic acid, L-(S)-lactate (8F8O, wheat carbons), and acetate (7T1Q, teal carbons) are shown, and zinc ions are shown as spheres in magenta (8F8O) and orange (7T1Q).

structure is composed of two polypeptide chains in the asymmetric unit, which form a dimer (Figure 1A). Each *Ab*DapE-SeMet chain consists of two domains: a catalytic domain comprising residues 1−177 and 299−378 and a dimerization domain comprising residues 178−298 (Figure 1A). Each *Ab*DapE-SeMet protomer retains two canonical and fully occupied dinuclear-Zn(II) binding sites, in which zinc ions are coordinated at site one by residues His68, Asp101, and Glu164 and at site two by residues Asp101, Glu136, and His350 (Figure 1B). As expected, these residues are conserved across all Gram-negative DapE enzymes examined (Figure S9).

The two *Ab*DapE-SeMet structures are nearly identical and overlay with a root-mean-square deviation (RMSD) of 0.23 Å across all atoms. Furthermore, one of the products of N^6-methyl-L,L-SDAP hydrolysis, succinate, is observed in identical positions in both structures (Figure 1C). The second product, N^6-methyl-L,L-DAP, is likely lost from the active site due to steric interactions from the additional *N*-methyl group and is instead exchanged for acetate in crystal 1 (7T1Q) derived from the crystallization buffer. In crystal 2, we observe L-(S)-lactate in the active site with the carboxylate in the same position as the acetate in crystal 1. We suspect that N^6-methyl-L,L-DAP was exchanged for citrate derived from the crystallization buffer and subsequently underwent X-ray induced degradation during the data collection process. The synchrotron X-ray induced degradation of amino acids and ligands is well precedented.[33] In our crystal, we hypothesize that degradation of citrate to lactate occurred via familiar loss of carbon dioxide and in addition the loss of acetate leading to lactate as shown in Scheme 2. A full mechanistic hypothesis is included in the Supporting Information as Scheme S1.

Interestingly, we observe only L-(S)-lactate bound to the active site, which would require an enantioselective hydrogen atom transfer to the 2-hydroxypropanoate radical. This agrees with the chirality of the active site and the preference for (S)-stereochemistry in the position occupied by lactate, which

Scheme 2. Hypothesized X-ray Induced Loss of Acetate and CO_2 Forming Lactate in the Active Site

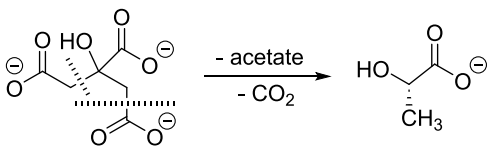

https://doi.org/10.1021/acsomega.3c08231
ACS Omega 2024, 9, 3905−3915

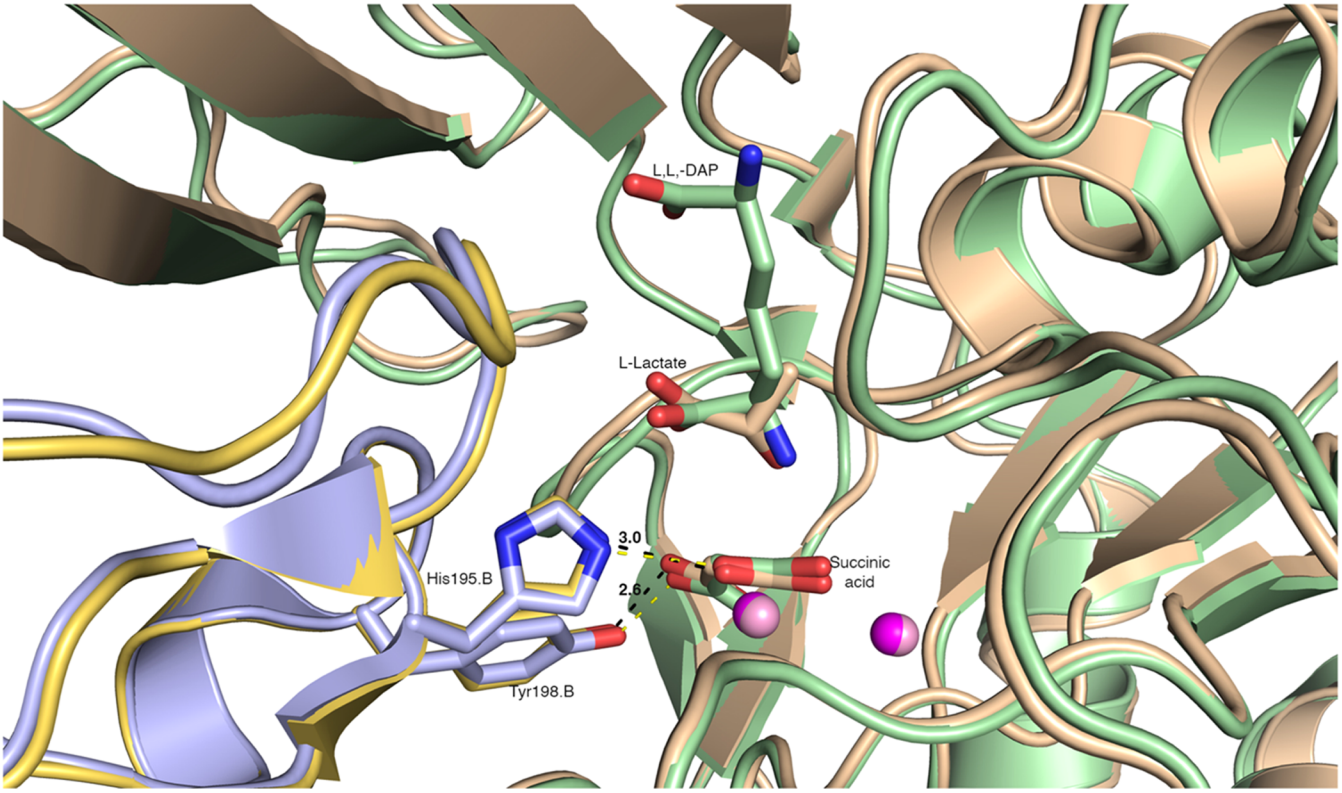

Figure 2. Close-up view of the active sites of superimposed structures of *Hi*DapE (PDB 5VO3, chain A pale green, symmetry-related chain of the dimer in pale violet) and *Ab*DapE (PDB 8F8O chain A wheat, chain B yellow). Residues His195 and Tyr198 of chain B from *Ab*DapE and corresponding residues from *Hi*DapE and products of the reactions are shown as sticks (carbons match the colors of the chains, oxygen in red, nitrogen in blue), and zinc shown as spheres (magenta for 8F8O and pink for 5VO3). Bonds between His195.B and Tyr198.B of *Ab*DapE and oxygen atoms of the succinate are shown by dashed lines with distances provided in angstroms.

corresponds to the (S)-stereochemistry of the substrates SDAP and N^6-methyl-L,L-SDAP.

Comparison of *Ab*DapE-SeMet with Homologues from *H. influenzae* and *N. meningitidis*. Upon binding of L,L,-SDAP to DapE, the catalytic domain shifts to obstruct access to the active site in a significant transition from the DapE "open" conformation to the "closed" conformation.[14] These changes bring two important residues, His195 and Tyr198, from the neighboring chain closer to the active site and help them directly interact with the substrate. We aligned the *Ab*DapE-SeMet structure to that of *Hi*DapE (5VO3, 58% identity) and compared the positions of reaction products in the active sites. The structures superimpose well with an RMSD of 0.87 Å (Figure 2). Close comparison of the *Ab*DapE-SeMet dinuclear Zinc(II) active site to that of *Hi*DapE shows that residues involved in substrate binding and catalysis are 100% conserved and almost all these residues are conserved across all Gram-negative DapE proteins (Figures 2 and S9,S10A). In our structures, specific residues from chain A, including Glu135, Arg179, Arg259, Gly325, and Thr326, and from chain B, including His195, Tyr198, and Asn246, form contacts with succinic acid, L-(S)-lactate and acetate (Figure S10B). Importantly, in agreement with what was previously observed for the *Hi*DapE closed-state structure,[14] the Zn(II) cluster, Arg179, and Gly325 from chain A, and His195 and Tyr198 of chain B form direct contacts with succinic acid. As expected, the distances between key residues His195 (3.0 Å) and Tyr198 (2.6 Å) and the oxygen atoms of succinic acid are also in agreement with the *Hi*DapE structure. Lastly, the positions of zinc ions and succinate are almost identical in these structures, and the position of L-(S)-lactate in *Ab*DapE-SeMet closely matches the position of the diaminopimelic moiety of the L-L-DAP product observed in the *Hi*DapE active site. We conclude that these conserved interactions between the reaction products and *Ab*DapE active site residues stabilize the protein in the closed conformation after substrate hydrolysis.

DapE Conformational Changes Result from Hinge Region Flexibility. We previously compared DapE structures available in the PDB and described the flexibility of DapE from different bacteria species.[16] At that time, there was only one closed ligand-bound structure known (PDB 5VO3) but, as noted above, the *Ab*DapE structures represent two new ligand-bound forms. An overlay of the *Nm*DapE (5UEJ) and *Hi*DapE (3IC1) structures highlights the open conformation of the dimer in ligand-free structures, whereas *Ab*DapE structures are more compact. The distance between C-terminal residues of $\alpha 3$ in open *Hi*DapE and *Nm*DapE structures averages 123 Å (Figure 3A) versus that in the closed *Ab*DapE structures, which is 108 Å (Figure 3B). These data support the finding that binding of a ligand to the active site stabilizes a specific quaternary structure, the closed conformation. Furthermore, alignment of the catalytic and dimerization domains of open and closed structures shows no significant changes in their conformations (Figure 3C). In contrast, alignment of the hinge regions of open and closed structures demonstrates the flexibility of this region, suggesting that changes in quaternary structure are determined by movements in the hinge region rather than changes in the structures of other domains (Figure

https://doi.org/10.1021/acsomega.3c08231
ACS Omega 2024, 9, 3905−3915

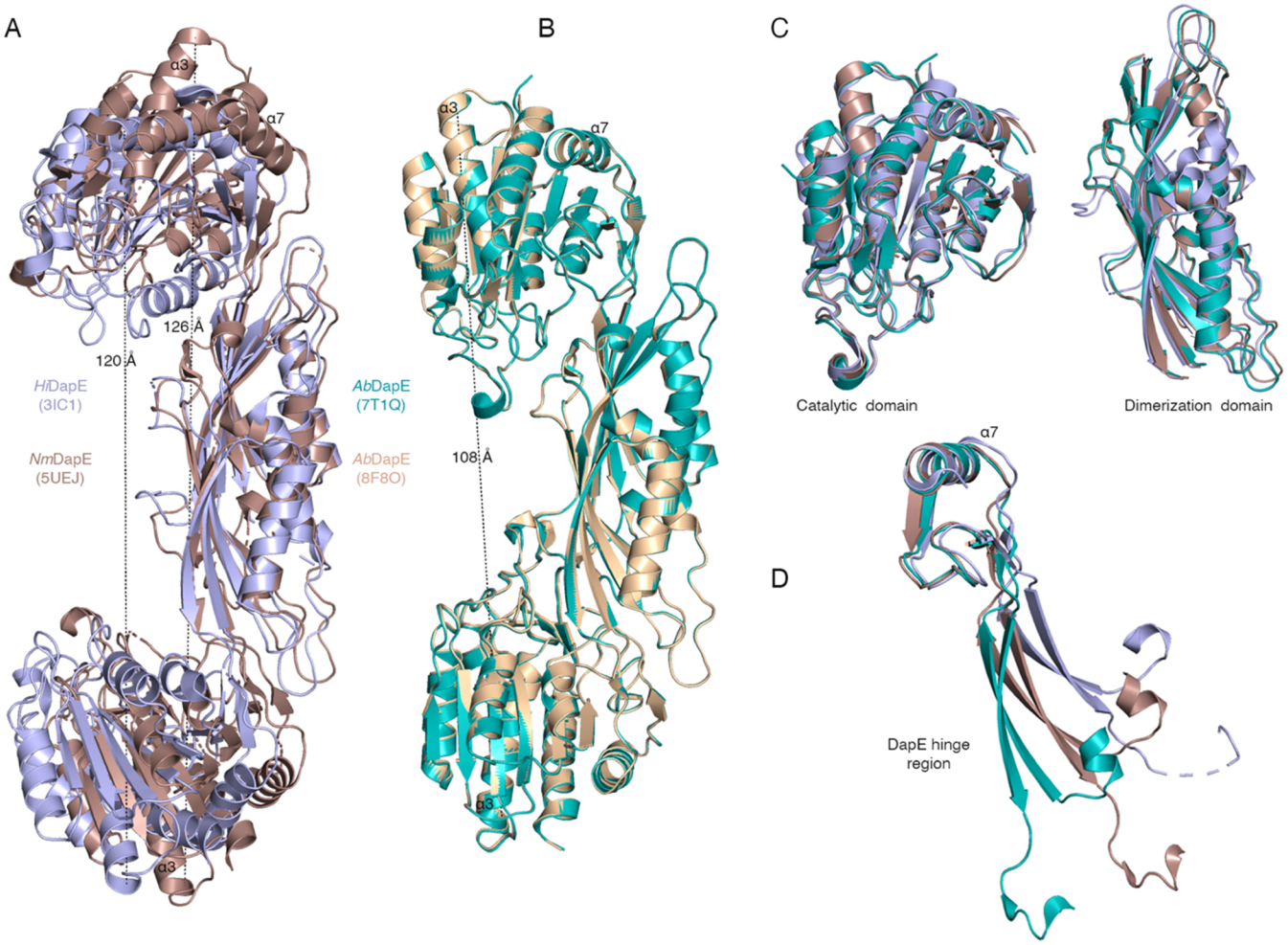

Figure 3. Closed and open states of DapE result from movement in the hinge region. Overlaps of (A) open *Nm*DapE and *Hi*DapE and (B) closed *Ab*DapE structures. The distances between c-terminal residues of α-helix 3 are shown with dashed lines. (C) Superimposed catalytic and dimerization domains of *Ab*DapE (7T1Q), *Hi*DapE, and *Nm*DapE. (D) Superimposed hinge regions of *Ab*DapE (7T1Q), *Hi*DapE, and *Nm*DapE. The α-helix 7 of the regions was aligned to emphasize movement of hinge residues. Coloring scheme is the same as in panels A and B.

3D). These overlays complement the analyses of DapE performed by Díaz-Sánchez.[34]

Mishra[35] very recently reported the binding energies of the products of DapE cleavage, with succinate bound very tightly (−25.87 and −22.26 kcal/mol in DapE monomer chains A and B, respectively), while DAP is less tightly bound (−19.14 kcal/mol and −17.51 kcal/mol in chains A and B, respectively). Moreover, he showed through molecular dynamics studies that DapE is very stable and remains closed with both products bound (starting with the products-bound structure PDB 5VO3), but removing both products allows DapE to open in a molecular dynamics run on the order of about 44 ns. The crystal structures we are reporting herein retain succinic acid in the active site, suggesting that this product is key for stabilizing the closed conformation of DapE.

■ CONCLUSIONS

We have enzymatically and structurally characterized DapE from *A. baumannii*, an important ESKAPE pathogen that exhibits significant antibiotic resistance. We assessed three known inhibitors of *Hi*DapE: captopril, lithium sulfate, and 1-acetyl-5-chloro-N-isopentylindoline-6-sulfonamide for inhibition of *Ab*DapE in our ninhydrin-based assay.[14] Captopril inhibited *Ab*DapE with an IC_{50} value of 1.2 μM, comparable to the IC_{50} of 3.3 μM for captopril versus *Hi*DapE. Sulfate inhibited *Ab*DapE with an IC_{50} of 13.5 mM, comparable to the IC_{50} of 23.9 mM for HiDapE, but the indoline sulfonamide did not measurably inhibit *Ab*DapE, yet has an IC_{50} of 54.0 μM for *Hi*DapE. This suggests that a broad-spectrum DapE inhibitor may be inaccessible. However, broad-spectrum antibiotics can disrupt the composition of a healthy microbiome, so greater antibiotic specificity may prove to be an advantage.

Both *Ab*DapE and a SeMet derivative were characterized with a TSA using captopril and sulfate as ligands and compared to those of the more thoroughly studied *Hi*DapE. *Ab*DapE exhibited biphasic transitions at 41.9 °C and at T_m2 at 63.2 °C that were somewhat lower than those transitions for *Hi*DapE (T_m1 = 51.5 °C and T_m2 = 78.2 °C). In contrast, *Ab*DapE-SeMet exhibited a single phase transition, with T_m at 65.2 °C; the higher temperature is consistent with the known stabilization of proteins by substitution of methionine by SeMet. The negative shift in T_m2 may indicate that captopril and sulfate ions destabilize *Hi*DapE by binding more tightly to the unfolded molten globular state of the enzyme,[36−38] thus stabilizing the more globular state. In general, it is risky to make conclusions about T_m2, since having passed T_m1, the enzyme is no longer in its native state and is in some partly globular state.

https://doi.org/10.1021/acsomega.3c08231
ACS Omega 2024, 9, 3905−3915

Díaz-Sánchez et al. reported thermal shift (also referred to as thermofluorescence, TF) studies for DapE from *E. faecium* (*Ef*DapE) and *E. coli* (*Ec*DapE), and they observed an apparent melt temperature (app. T_m) of 43.0 ± 0.5 °C for *Ef*DapE and 42.0 ± 0.6 °C for *Ec*DapE.[36] Further, they discovered two new inhibitors of DapE, disulfiram and orphenadrine, and reported a lowering of the T_m values of DapE in the presence of those inhibitors, whereas we observed a stabilization of T_m1 for *Hi*DapE and *Ab*DapE with both captopril and sulfate. While it is most common for a ligand binding to a protein to stabilize the structure and therein raise the T_m to higher temperatures, the lowering of T_m through destabilization has been observed as well.[39−41]

Differences in potencies of inhibitors as well as differences in thermal shift may be due to the somewhat lower homology between *Ab*DapE and *Hi*DapE (58.2%). By comparison with another important infectious bacteria species, *Mycobacterium tuberculosis* DapE (*Mt*DapE) has only 24.4% homology with *Hi*DapE, and hence, its structure−activity relationship should be quite distinct.

As previously noted, the native *Hi*DapE and *Ab*DapE enzymes exhibit two melt temperatures. We hypothesize that T_m1 may indicate the denaturation of the dimer, and T_m2 involves the denaturation of the dissociated monomer. These two temperatures corresponding to denaturation are consistent with our previously reported circular dichroism studies,[7] which revealed that the α-helices of the enzyme begin to denature between 50 and 60 °C, corresponding to T_m1, and undergo further denaturation after 2−3 min of heating at 80 °C (≤10% of α-helices activity remaining), corresponding to T_m2. It has been reported[32] that substitution of Met with SeMet stabilizes proteins; it is curious that SeMet has two T_m values, whereas *Ab*DapE-SeMet exhibits only one T_m value.

Attempts to cocrystallize *Ab*DapE with the modified substrate N^6−methyl-L,L-SDAP substrate resulted in two *Ab*DapE structures in the complex with reaction products, succinic acid and L-(S)-lactate (8F8O) and acetate (7T1Q). These new DapE structures are the only closed DapE conformers reported in the literature except for one previously reported structure of *Hi*DapE in complex with succinic and diaminopimelic (DAP) acids (5VO3).[14] Comparison of these structures shows that the position of succinic acid is retained in both *H. influenzae* and *A. baumannii* DapE enzymes. Furthermore, interactions between succinic acid, zinc ions, and key residues of DapE are conserved in our structures, and these interactions help to stabilize the closed conformation after catalysis. These interactions reveal conformational changes in the DapE hinge region that are noteworthy when comparing the closed and open conformers. Lastly, despite expulsion of the N^6-methyl-L,L-DAP product from the *Ab*DapE active site, carboxylates of L-(S)-lactate and acetate in *Ab*DapE structures are in the same position as the carboxylate of DAP in *Hi*DapE. These data support conservation of the DapE mechanism in another pathogenic bacterium, specifically an ESKAPE pathogen, further reason for continued efforts in developing novel therapeutics that target DapE.

■ ASSOCIATED CONTENT

Supporting Information

The Supporting Information is available free of charge at https://pubs.acs.org/doi/10.1021/acsomega.3c08231.

X-ray collection and refinement statistics; plots of inhibition by captopril, sulfate (Li_2SO_4), 1-acetyl-5-chloro-N-isopentylindoline-6-sulfonamide, and TSA plots (PDF)

Accession Codes

Protein Data Bank: PDB codes 7T1Q and 8F8O

■ AUTHOR INFORMATION

Corresponding Author

Daniel P. Becker − *Department of Chemistry and Biochemistry, Loyola University Chicago, Chicago, Illinois 60660, United States;* orcid.org/0000-0001-9392-0460; Phone: 773-508-3089; Email: dbecke3@luc.edu

Authors

Emma H. Kelley − *Department of Chemistry and Biochemistry, Loyola University Chicago, Chicago, Illinois 60660, United States*

George Minasov − *Department of Microbiology-Immunology, Northwestern University, Feinberg School of Medicine, Chicago, Illinois 60611, United States; Center for Structural Biology of Infectious Diseases, Northwestern University, Feinberg School of Medicine, Chicago, Illinois 60611, United States*

Katherine Konczak − *Department of Chemistry and Biochemistry, Loyola University Chicago, Chicago, Illinois 60660, United States;* orcid.org/0000-0002-2025-0475

Ludmilla Shuvalova − *Department of Pharmacology, Northwestern University, Feinberg School of Medicine, Chicago, Illinois 60611, United States*

Joseph S. Brunzelle − *Northwestern Synchrotron Research Center, Life Sciences Collaborative Access Team, Northwestern University, Argonne, Illinois 60439, United States*

Shantanu Shukla − *Department of Microbiology-Immunology, Northwestern University, Feinberg School of Medicine, Chicago, Illinois 60611, United States; Center for Structural Biology of Infectious Diseases, Northwestern University, Feinberg School of Medicine, Chicago, Illinois 60611, United States*

Megan Beulke − *Department of Chemistry and Biochemistry, Loyola University Chicago, Chicago, Illinois 60660, United States*

Teerana Thabthimthong − *Department of Chemistry and Biochemistry, Loyola University Chicago, Chicago, Illinois 60660, United States*

Kenneth W. Olsen − *Department of Chemistry and Biochemistry, Loyola University Chicago, Chicago, Illinois 60660, United States*

Nicole L. Inniss − *Department of Microbiology-Immunology, Northwestern University, Feinberg School of Medicine, Chicago, Illinois 60611, United States; Center for Structural Biology of Infectious Diseases, Northwestern University, Feinberg School of Medicine, Chicago, Illinois 60611, United States*

Karla J. F. Satchell − *Department of Microbiology-Immunology, Northwestern University, Feinberg School of Medicine, Chicago, Illinois 60611, United States; Center for Structural Biology of Infectious Diseases, Northwestern University, Feinberg School of Medicine, Chicago, Illinois 60611, United States;* orcid.org/0000-0003-3274-7611

Complete contact information is available at:

https://pubs.acs.org/10.1021/acsomega.3c08231

Author Contributions

[#]E.H.K. and G.M. contributed equally to this work.

Funding

This research was supported in part by the National Institutes for Allergies and Infectious Diseases of the National Institutes of Health department of the Health and Human Services under contracts HHSN272201700060C and 75N93022C00035. This research used resources of the Advanced Photon Source, a U.S. Department of Energy (DOE) Office of Science User Facility operated for the DOE Office of Science by Argonne National Laboratory under contract no. DE-AC02-06CH11357. Use of the LS-CAT Sector 21 was supported by the Michigan Economic Development Corporation and the Michigan Technology Tri-Corridor (grant 085P1000817).

Notes

The authors declare no competing financial interest.

■ ACKNOWLEDGMENTS

The authors thank Ievgeniia Dubrovska for freezing crystals that led to the *A. baumannii* DapE structures. The authors also thank Sergii Pshenychnyi at Northwestern University for protein purification.

■ REFERENCES

(1) *Antibacterial Agents in Clinical Development: An Analysis of the Antibacterial Clinical Development Pipeline, Including Tuberculosis*; World Health Organization, 2017.

(2) Mulani, M. S.; Kamble, E. E.; Kumkar, S. N.; Tawre, M. S.; Pardesi, K. R. Emerging strategies to combat ESKAPE pathogens in the era of antimicrobial resistance: a review. *Front. Microbiol.* **2019**, *10*, No. 539.

(3) Peleg, A. Y.; Seifert, H.; Paterson, D. L. *Acinetobacter baumannii*: emergence of a successful pathogen. *Clin. Microbiol. Rev.* **2008**, *21*, 538−582.

(4) Muduli, S.; Karmakar, S.; Mishra, S. The coordinated action of the enzymes in the L-lysine biosynthetic pathway and how to inhibit it for antibiotic targets. *Biochim. Biophys. Acta, General Subj.* **2023**, *1867*, No. 130320.

(5) Gillner, D. M.; Becker, D. P.; Holz, R. C. Lysine biosynthesis in bacteria: a metallodesuccinylase as a potential antimicrobial target. *JBIC, J. Biol. Inorg. Chem.* **2013**, *18*, 155−163.

(6) Scapin, G.; Blanchard, J. S. Enzymology of Bacterial Lysine Biosynthesis. In *Advances in Enzymologyand Related Areas of Molecular Biology*; John Wiley & Sons, Inc., 2006; pp 279−324.

(7) Heath, T. K.; Lutz, M. R., Jr; Reidl, C. T.; Guzman, E. R.; Herbert, C. A.; Nocek, B. P.; Holz, R. C.; Olsen, K. W.; Ballicora, M. A.; Becker, D. P. Practical spectrophotometric assay for the dapE-encoded N-succinyl-L, L-diaminopimelic acid desuccinylase, a potential antibiotic target. *PLoS One* **2018**, *13*, No. e0196010.

(8) Karita, M.; Etterbeek, M. L.; Forsyth, M. H.; Tummuru, M. K. R.; Blaser, M. J. Characterization of *Helicobacter pylori* dapE and construction of a conditionally lethal dapE mutant. *Infect. Immun.* **1997**, *65*, 4158−4164.

(9) Pavelka, M. S., Jr.; Jacobs, W. R., Jr. Biosynthesis of diaminopimelate, the precursor of lysine and a component of peptidoglycan, is an essential function of *Mycobacterium smegmatis*. *J. Bacteriol.* **1996**, *178*, 6496−6507.

(10) Badger, J.; Sauder, J. M.; Adams, J. M.; Antonysamy, S.; Bain, K.; Bergseid, M. G.; Buchanan, S. G.; Buchanan, M. D.; Batiyenko, Y.; Christopher, J. A.; et al. Structural analysis of a set of proteins resulting from a bacterial genomics project. *Proteins: Struct., Funct., Bioinf.* **2005**, *60*, 787−796.

(11) Nocek, B. P.; Gillner, D. M.; Fan, Y.; Holz, R. C.; Joachimiak, A. Structural Basis for Catalysis by the Mono- and Dimetalated Forms of the dapE-Encoded N-succinyl-L,L-Diaminopimelic Acid Desuccinylase. *J. Mol. Biol.* **2010**, *397*, 617−626.

(12) Starus, A.; Nocek, B.; Bennett, B.; Larrabee, J. A.; Shaw, D. L.; Sae-Lee, W.; Russo, M. T.; Gillner, D. M.; Makowska-Grzyska, M.; Joachimiak, A.; Holz, R. C. Inhibition of the dapE-Encoded N-Succinyl-L,L-diaminopimelic Acid Desuccinylase from *Neisseria meningitidis* by L-Captopril. *Biochemistry* **2015**, *54*, 4834−4844.

(13) Gillner, D. M.; Bienvenue, D. L.; Nocek, B. P.; Joachimiak, A.; Zachary, V.; Bennett, B.; Holz, R. C. The dapE-encoded N-succinyl-L,L-diaminopimelic acid desuccinylase from *Haemophilus influenzae* contains two active-site histidine residues. *JBIC, J. Biol. Inorg. Chem.* **2009**, *14*, 1−10.

(14) Nocek, B.; Reidl, C.; Starus, A.; Heath, T.; Bienvenue, D.; Osipiuk, J.; Jedrzejczak, R. P.; Joachimiak, A.; Becker, D. P.; Holz, R. C. Structural Evidence for a Major Conformational Change Triggered by Substrate Binding in DapE Enzymes: Impact on the Catalytic Mechanism. *Biochemistry* **2018**, *57*, 574.

(15) Dutta, D.; Mishra, S. Structural and mechanistic insight into substrate binding from the conformational dynamics in apo and substrate-bound DapE enzyme. *Phys. Chem. Chem. Phys.* **2016**, *18*, 1671−1680.

(16) Kochert, M.; Nocek, B. P.; Habeeb Mohammad, T. S.; Gild, E.; Lovato, K.; Heath, T. K.; Holz, R. C.; Olsen, K. W.; Becker, D. P. Atomic-Resolution 1.3 Å Crystal Structure, Inhibition by Sulfate, and Molecular Dynamics of the Bacterial Enzyme DapE. *Biochemistry* **2021**, *60*, 908−917.

(17) Minor, W.; Cymborowski, M.; Otwinowski, Z.; Chruszcz, M. HKL-3000: the integration of data reduction and structure solution−from diffraction images to an initial model in minutes. *Acta Crystallogr., Sect. D: Biol. Crystallogr.* **2006**, *62*, 859−866.

(18) McCoy, A. J.; Grosse-Kunstleve, R. W.; Adams, P. D.; Winn, M. D.; Storoni, L. C.; Read, R. J. Phaser crystallographic software. *J. Appl. Crystallogr.* **2007**, *40*, 658−674.

(19) Winn, M. D.; Ballard, C. C.; Cowtan, K. D.; Dodson, E. J.; Emsley, P.; Evans, P. R.; Keegan, R. M.; Krissinel, E. B.; Leslie, A. G.; McCoy, A.; et al. Overview of the CCP4 suite and current developments. *Acta Crystallogr., Sect. D: Biol. Crystallogr.* **2011**, *67*, 235−242.

(20) Murshudov, G. N.; Skubák, P.; Lebedev, A. A.; Pannu, N. S.; Steiner, R. A.; Nicholls, R. A.; Winn, M. D.; Long, F.; Vagin, A. A. REFMAC5 for the refinement of macromolecular crystal structures. *Acta Crystallogr., Sect. D: Biol. Crystallogr.* **2011**, *67*, 355−367.

(21) Emsley, P.; Cowtan, K. Coot: model-building tools for molecular graphics. *Acta Crystallogr., Sect. D: Biol. Crystallogr.* **2004**, *60*, 2126.

(22) Langer, G.; Cohen, S. X.; Lamzin, V. S.; Perrakis, A. Automated macromolecular model building for X-ray crystallography using ARP/wARP version 7. *Nat. Protoc.* **2008**, *3*, 1171−1179.

(23) Chen, V. B.; Davis, I. W.; Richardson, D. C. KING (Kinemage, Next Generation): a versatile interactive molecular and scientific visualization program. *Protein Sci.* **2009**, *18*, 2403−2409.

(24) Williams, C. J.; Headd, J. J.; Moriarty, N. W.; Prisant, M. G.; Videau, L. L.; Deis, L. N.; Verma, V.; Keedy, D. A.; Hintze, B. J.; Chen, V. B.; et al. MolProbity: More and better reference data for improved all-atom structure validation. *Protein Sci.* **2018**, *27*, 293−315.

(25) Karayannis, M. I.; Samios, D. N.; Gousetis, C. A study of the molar absorptivity of ascorbic acid at different wavelengths and pH values. *Anal. Chim. Acta* **1977**, *93*, 275−279.

(26) Altschul, S. F.; Gish, W.; Miller, W.; Myers, E. W.; Lipman, D. J. Basic local alignment search tool. *J. Mol. Biol.* **1990**, *215*, 403−410.

(27) Sievers, F.; Wilm, A.; Dineen, D.; Gibson, T. J.; Karplus, K.; Li, W.; Lopez, R.; McWilliam, H.; Remmert, M.; Soding, J.; Thompson, J. D.; Higgins, D. G. Fast, scalable generation of high-quality protein multiple sequence alignments using Clustal Omega. *Mol. Syst. Biol.* **2011**, *7*, No. 539.

(28) Gouet, P. ESPript/ENDscript: extracting and rendering sequence and 3D information from atomic structures of proteins. *Nucleic Acids Res.* **2003**, *31*, 3320−3323.

(29) Bhayani, J. A.; Ballicora, M. A. Determination of dissociation constants of protein ligands by thermal shift assay. *Biochem. Biophys. Res. Commun.* **2022**, *590*, 1−6.
(30) Gillner, D.; Armoush, N.; Holz, R. C.; Becker, D. P. Inhibitors of bacterial N-succinyl-L,L-diaminopimelic acid desuccinylase (DapE) and demonstration of in vitro antimicrobial activity. *Bioorg. Med. Chem. Lett.* **2009**, *19*, 6350−6352.
(31) Reidl, C. T.; Heath, T. K.; Darwish, I.; Torrez, R. M.; Moore, M.; Gild, E.; Nocek, B. P.; Starus, A.; Holz, R. C.; Becker, D. P. Indoline-6-Sulfonamide Inhibitors of the Bacterial Enzyme DapE. *Antibiotics* **2020**, *9*, No. 595.
(32) Gassner, N. C.; Baase, W. A.; Hausrath, A. C.; Matthews, B. W. Substitution with selenomethionine can enhance the stability of methionine-rich proteins. *J. Mol. Biol.* **1999**, *294*, 17−20.
(33) Burmeister, W. P. Structural changes in a cryo-cooled protein crystal owing to radiation damage. *Acta Crystallogr., D: Biol. Crystallogr.* **2000**, *56*, 328−341.
(34) Díaz-Sánchez, Á. G.; Terrazas-López, M.; Aguirre-Reyes, L. G.; Lobo-Galo, N.; Álvarez-Parrilla, E.; Martínez-Martínez, A. Aspectos estructurales y funcionales de la N-Succinil-L, L-diaminopimelato desuccinilasa, una enzima clave para el crecimiento bacteriano y un blanco para el control antimicrobiano. *TIP, Rev. Espec. Cienc. Quim.-Biol.* **2019**, *22*. DOI: 10.22201/fesz.23958723e.2019.0.191.
(35) Muduli, S.; Mishra, S. Ligands-Induced Open-Close Conformational Change during DapE Catalysis: Insights from Molecular Dynamics Simulations. *Proteins: Struct., Funct., Bioinf.* **2023**, *91*, 781−797, DOI: 10.1002/prot.26466.
(36) Terrazas-López, M.; Lobo-Galo, N.; Aguirre-Reyes, L. G.; Bustos-Jaimes, I.; Marcos-Víquez, J. Á.; González-Segura, L.; Díaz-Sánchez, Á. G. Interaction of N-succinyl diaminopimelate desuccinylase with orphenadrine and disulfiram. *J. Mol. Struct.* **2020**, *1222*, No. 128928.
(37) Bhusal, R. P.; Patel, K.; Kwai, B. X.; Swartjes, A.; Bashiri, G.; Reynisson, J.; Sperry, J.; Leung, I. K. Development of NMR and thermal shift assays for the evaluation of *Mycobacterium tuberculosis* isocitrate lyase inhibitors. *MedChemComm* **2017**, *8*, 2155−2163.
(38) Cimmperman, P.; Baranauskienė, L.; Jachimovičiūtė, S.; Jachno, J.; Torresan, J.; Michailovienė, V.; Matulienė, J.; Sereikaitė, J.; Bumelis, V.; Matulis, D. A quantitative model of thermal stabilization and destabilization of proteins by ligands. *Biophys. J.* **2008**, *95*, 3222−3231.
(39) Velasco-García, R.; Zaldívar-Machorro, V. J.; Mújica-Jiménez, C.; González-Segura, L.; Muñoz-Clares, R. A. Disulfiram irreversibly aggregates betaine aldehyde dehydrogenase—a potential target for antimicrobial agents against *Pseudomonas aeruginosa*. *Biochem. Biophys. Res. Commun.* **2006**, *341*, 408−415.
(40) Douse, C. H.; Vrielink, N.; Wenlin, Z.; Cota, E.; Tate, E. W. Targeting a dynamic protein−protein interaction: fragment screening against the malaria myosin A motor complex. *ChemMedChem* **2015**, *10*, 134−143.
(41) Kabir, A.; Honda, R. P.; Kamatari, Y. O.; Endo, S.; Fukuoka, M.; Kuwata, K. Effects of ligand binding on the stability of aldo−keto reductases: Implications for stabilizer or destabilizer chaperones. *Protein Sci.* **2016**, *25*, 2132−2141.

https://doi.org/10.1021/acsomega.3c08231
ACS Omega 2024, 9, 3905−3915